

Effect of low-temperature annealing on the void-induced microstructure in amorphous silicon: A computational study

Durga Paudel,¹ Raymond Atta-Fynn,² David A. Drabold,³ and Parthapratim Biswas¹

¹*Department of Physics and Astronomy, The University of Southern Mississippi, Hattiesburg, MS 39406**

²*Department of Physics, University of Texas, Arlington, TX 76019*

³*Department of Physics and Astronomy, Ohio University, Athens, Ohio 45701*

We present a computational study of the void-induced microstructure in amorphous silicon (*a*-Si) by generating ultra-large models of *a*-Si with a void-volume fraction of 0.3%, as observed in small-angle x-ray scattering (SAXS) experiments. The relationship between the morphology of voids and the intensity of scattering in SAXS has been studied by computing the latter from the Fourier transform of the reduced pair-correlation function and the atomic-form factor of amorphous silicon. The effect of low-temperature (≤ 600 K) annealing on the scattering intensities and the microstructure of voids has been addressed, with particular emphasis on the shape and size of the voids, by studying atomic rearrangements on the void surfaces and computing the average radius of gyration of the voids from the spatial distribution of surface atoms and the intensity plots in the Guinier approximation. The study suggests that low-temperature annealing can lead to considerable restructuring of void surfaces, which is clearly visible from the three-dimensional shape of the voids but it may not necessarily reflect in one-dimensional scattering-intensity plots.

I. INTRODUCTION

The microstructure of small- and large-scale inhomogeneities, such as multi-vacancies and voids, plays an important role in the determination of structural and optoelectronic properties of pure and hydrogenated amorphous silicon¹. The presence of voids in amorphous silicon (*a*-Si) and germanium (*a*-Ge) was postulated in the late 1960s by Brodsky and Title² and Moss and Graczyk,³ with the aid of electron spin resonance (ESR) and small-angle electron diffraction measurements, respectively, to explain the low mass density of amorphous Si/Ge (by about 10–15%) from their crystalline counterparts. In the intervening decades, a number of experimental techniques, ranging from small-angle x-ray scattering (SAXS),⁴ spectroscopic ellipsometry (SE), Fourier transform infrared spectroscopy (FTIR),⁵ and effusion of hydrogen and implanted-helium measurements⁶ in *a*-Si:H to nuclear magnetic resonance (NMR),⁷ provided an impressive database of experimental information on structural properties of *a*-Si and its hydrogenated counterpart. By contrast, until recently,⁸ computational efforts^{9–12} to address structural and electronic properties of *a*-Si have been mostly limited to results obtained from small atomistic models, consisting of a few to several hundreds of atoms, depending upon the quantum-mechanical or classical nature of atomic interactions employed in building those models. Thus, the computational modeling of large-scale inhomogeneities in amorphous networks, such as voids in *a*-Si and *a*-Ge, were particularly hindered in the past due to the absence of large realistic models, which were needed to take into account the size and the number density of the voids, as observed in SAXS, NMR and FTIR studies. Since voids are nanoscale inhomogeneities, with a diameter ranging from 10–40 Å and a void-volume fraction of 0.1–0.4%, it is necessary to produce ultra-large models, consisting of 10^5 atoms or more, so that the models are not only experimentally compliant but also statistically reliable and capable of producing configurational-averaged values of physical properties. In this communication, we address the structure of void-induced

morphology in *a*-Si by carrying out realistic simulations of voids, using classical molecular-dynamics simulations.

Of particular interest is the evolution of the microstructure of voids in *a*-Si/*a*-Si:H, induced by thermal annealing. While it is known that annealing at low temperature increases structural ordering in *a*-Si, as observed in Raman spectroscopy,¹³ the effect of annealing on the shape and size of the voids is still largely unknown. Since the restructuring of atoms in the vicinity of void surfaces, especially in *a*-Si:H, is intrinsically connected with the photovoltaic behavior of *a*-Si:H-based solar devices, computational studies of the relaxation behavior of atoms on and near the void surfaces are of paramount importance. Here, we present a quantitative study of characterization of void shapes and sizes upon low-temperature annealing by examining the spatial distributions of void-surface atoms and computing the scattering intensity in SAXS, produced by the voids of evolving shape present in the models.

The rest of the paper is as follows. In sec. II, we provide a brief description of the computational method to obtain atomistic models of *a*-Si via classical molecular-dynamics (MD) simulations using the modified Stillinger-Weber potential.¹⁴ The computation of the scattering intensity in SAXS using the MD models as the structural basis is also described in this section. Section III discusses the results of low temperature annealing, from 300 K to 600 K, on the void surfaces with an emphasis on the shape of the scattering intensity plots. The conclusions of our work are presented in sec. IV.

II. COMPUTATIONAL METHOD

Since scattering contributions in SAXS chiefly originate from the small wave-vector region ($k \leq 1 \text{ \AA}^{-1}$), it is essential to extract information on the extended-scale inhomogeneities by generating large models of *a*-Si for realistic simulation of scattering intensity in the small-angle region. Toward that end, we generated two independent *a*-Si models (M1 and M2), consisting of 262 400 atoms in a cubic supercell of length

176.123 Å, using the modified Stillinger-Weber potential¹⁴ via molecular-dynamics (MD) simulations in canonical ensembles. The MD simulations comprised the following steps: a) equilibration of an initial random configuration at 1800 K for 40 ps; b) gradual cooling of the equilibrated system from 1800 K to 300 K in steps of 100 K per 25 ps so that the total simulation time is 415 ps per cooling cycle; c) repetition of step (b) for up to 40 cycles until a high-quality amorphous network could form, which was characterized by a narrow bond-angle distribution and a small percentage of coordination defects; d) total-energy relaxations of the system at 300 K, using the limited-memory BFGS method,¹⁵ to obtain the nearest local minimum-energy configuration.

In order to study the temperature dependence of SAXS intensity and void shape, we generated four additional models from M1 and M2 by introducing ellipsoidal voids such that the total void-volume fraction, f_v , corresponds to 0.3%, as observed in experiments.¹⁶ The ellipsoidal voids were generated randomly so that they were sparsely distributed within amorphous networks with a minimum surface-to-surface distance of 6 Å between any two neighboring voids. An axial ratio of $a : b : c = 0.5 : 1 : 2$, with a length scale of $b = 6$ Å, was employed to generate ellipsoidal voids and the silicon atoms in the region between x and $x + d$, where $x = (a, b, c)$ and $d = 2.8$ Å, were marked as surface atoms in order to monitor the evolution of void shape upon annealing and relaxation. Two independent sets of models were studied to examine the effect of annealing on void shape and the intensity of scattering at 400 K and 600 K. The corresponding relaxed models were also examined in our work for a comparison.

The computation of scattering intensity in SAXS follows directly from the static structure factor, $S(k)$, and the atomic-form factor, $f(k)$, of *a*-Si. By invoking the homogeneous approximation, and subtracting the contribution coming from $k = 0$, the structure factor can be written as,

$$S(k) = 1 + \frac{1}{k} \int_0^{R_c} G(r) \sin kr \, dr. \quad (1)$$

Here, $G(r)$ is the reduced pair-correlation function (PCF) and k is the magnitude of wave-vector transfer, $k = 4\pi \sin(\theta)/\lambda$, where 2θ is the scattering angle and λ is the wavelength of x-ray. The upper limit of the integral in Eq. (1) is chosen so that $G(r)$ can be neglected for $r > R_c = 30$ Å. Denoting $f(k)$ as the atomic-form factor, the scattering intensity, $I(k)$, can be written as, $I(k) = \frac{1}{N} |f(k)|^2 S(k)$, where N is the total number of atoms.

III. RESULTS AND DISCUSSIONS

Table I lists the characteristic structural properties of M1 and M2 models, obtained from molecular-dynamics (MD) simulations. Given the ultra-large size of the models, it is remarkable that the concentration of coordination defects and the root-mean-square (RMS) deviation of bond angles are less than 2.4% and 10°, respectively. Figure 1 shows the static structure factor of the simulated models, averaged over M1 and M2 models, along with the experimental structure-factor

TABLE I. Structural properties of simulated models of amorphous silicon: N , ρ , C_4 , C_3 , r_{avg} , θ_{avg} , and $\Delta\theta$ are the size of the simulation cell, total number of atoms, density, four-fold coordination, three-fold coordination, average bond length, average bond angle, and the RMS deviation of the bond angles, respectively.

Model	N	ρ (g/cm ³)	C_4 (%)	C_3 (%)	r_{avg} (Å)	θ_{avg}	$\Delta\theta$
M1	262 400	2.24	97.65	1.27	2.39	109.24°	9.10°
M2	262 400	2.24	97.71	1.27	2.39	109.25°	9.08°

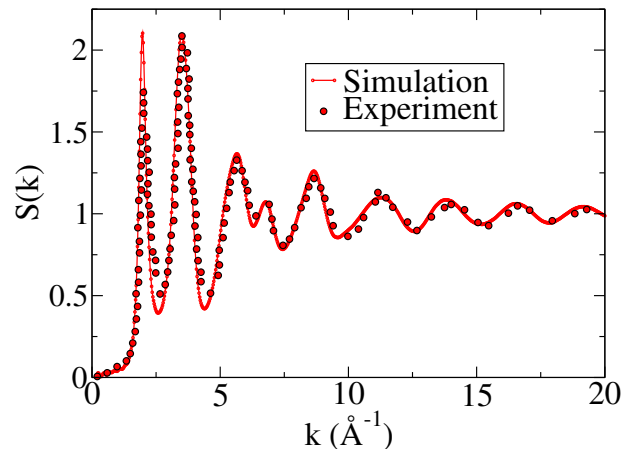


FIG. 1. The static structure factor of *a*-Si from simulations and experiments. The simulation data were averaged over M1 and M2 models. Experimental data correspond to annealed samples of *a*-Si from Ref. 17.

data from wide-angle x-ray diffraction measurements.¹⁷ The simulated values of the structure factor match closely with the experimental data, indicating that the models are not only fully consistent with two- and three-body correlation functions but also have a low concentration of coordination defects. To our knowledge, these ultra-large models are among the very best of *a*-Si models, from classical MD simulations, with 10⁵ or more atoms so far reported in the literature.

The effect of low-temperature annealing on the shape and size of the voids was studied by analyzing the results from real and reciprocal spaces. Figure 2 depicts the evolution of an ellipsoidal void at 400 K and 600 K, along with the original shape, all superimposed on each other. The distorted ellipsoidal surfaces observed at 400 K and 600 K are shown in green and red colors, respectively, whereas the original void surface is shown in blue color. The striking color patches, which originate from the superposition of three ellipsoidal surfaces, are reflective of the degree of reconstruction of the surface at 400 K (green) and 600 K (red). These surfaces were generated from the position coordinates of the respective void-surface atoms, using an identical set of iso-surface parameters in VMD software.¹⁸ To obtain a quantitative estimate of the degree of surface reconstruction, the distributions of atomic displacements (u) of the surface atoms of the ellipsoidal void at 600 K and 400 K are plotted in Fig. 3. While it is evident from Fig. 3 that majority of the surface atoms have displaced from their original position by a distance of 0–0.75 Å, a small

number of atoms have moved more than 1.0 \AA , causing considerable restructuring of the void surface. This observation has been found to be true for other ellipsoidal voids as well.

While an analysis of the three-dimensional distribution of atoms clearly reveals atomic rearrangements on void surfaces, a question of great importance, from the point of view of SAXS, is to what extent these temperature-induced structural changes can be reflected in $I(k)$ -vs- k plots. Since SAXS essentially provides *scalar* information or *one-dimensional* physical quantities, such as scattering intensities and the average radius of gyration of the voids in the Guinier approximation,¹⁹ it is pertinent to examine whether these scalar quantities are sensitive to structural changes observed on the void surfaces. Figure 4 shows the scattering intensities obtained from the original model with voids (blue) and the corresponding annealed models at 600 K (red) and 400 K (green). For comparison, we have also included the intensity values obtained from the original model with voids (blue) and without voids (black) before annealing. A few observations immediately follow from Fig. 4. First, an excess of small-angle scattering is apparent in the computed values of the scattering intensity from the models with voids (red/green/blue), compared with the one with no voids (black). Second, the variation of the scattering intensity in the presence of voids is mostly pronounced in the small- k region below 0.25 \AA^{-1} . Since the wave-vector region below 0.1 \AA^{-1} is not very reliable, owing to the presence of numerical noise at large distances in $G(r)$ (see Eq. 1), it would not be inappropriate to conclude that the changes are somewhat weakly reflected in the intensity plots as far as our simulations are concerned. Third, it appears that the scattering plot at 600 K (red) is somewhat smoothed out compared to the one at 400 K (green), which can be attributed to the temperature-induced improved local ordering in the network, especially in the vicinity of the void regions. Finally, the minor changes in the shape of the intensity plot are consistent with the values of the radius of gyration, obtained from the *real-space* distribution of surface atoms.

Table II lists R_g values obtained from the spatial distribution of void-surface atoms at 400 K and 600 K, which are quite close to each other. On the other hand, the radius of gyration, r_g , obtained from the intensity plots in the Guinier approximation,¹⁹ shows a noticeable variation with temperature. Since the Guinier approximation entails expressing $I(k) \approx I(0) \exp(-k^2 r_g^2/3)$ in the limit $k \rightarrow 0$, and fitting the intensity values on a semi-log plot, $\ln I(k)$ -vs- k^2 , r_g values obtained from this approach are quite sensitive to the computed values of the intensity and the length of the small- k region employed in the calculations. Here, we have employed intensity values in the region $0.015 \leq k^2 \leq 0.16 \text{ \AA}^{-1}$, to obtain the r_g values listed in Table II. In Figs. 5 to 7, we have presented the corresponding shape, atomic displacements, and the values of the scattering intensities obtained by relaxing the annealed models at temperature 400 K and 600 K, respectively. Although considerable changes in the shape of the relaxed ellipsoidal void can be seen in Fig. 5, the scattering intensities in Fig. 7 appear to be not particularly susceptible to the changes observed on the void surfaces.

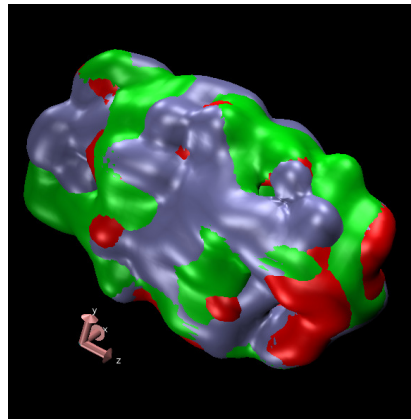


FIG. 2. The changing shape of an ellipsoidal void (M1-V5) in M1 model at two different annealing temperatures. Red and green colors correspond to the shape at temperature 600 K and 400 K, respectively, along with the original ellipsoid surface shown in blue color. The color patches are indicative of surface reconstruction, showing the evolving shape of the surface with temperature. The symbol M1-V5 indicates void number 5 in M1 model.

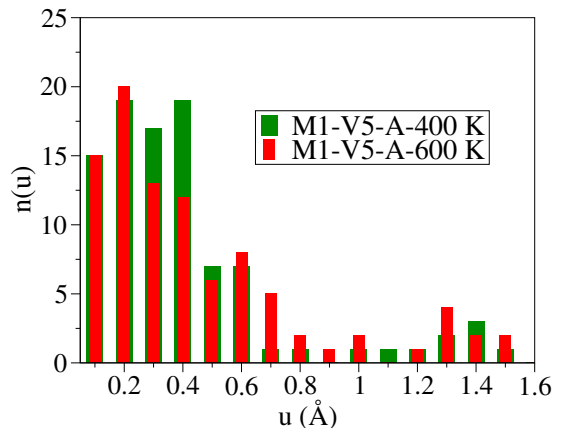


FIG. 3. The distributions of atomic displacements, $n(u)$, of the surface atoms on the ellipsoidal void (M1-V5) shown in Fig. 2. The distributions at 600 K and 400 K are shown in red and green colors, respectively.

IV. CONCLUSIONS

In this paper, we have studied the microstructure of nanometer-size voids, by simulating ultra-large models of *a*-Si, using classical molecular-dynamics simulations. The intensity of small-angle x-ray scattering, produced by ellipsoidal voids present in the models, is computed from the Fourier transform of the reduced pair-correlation function and the atomic-form factor of silicon in an effort to study the effect of low-temperature annealing of up to 600 K on the morphology, especially the shape and size, of the voids. Our study shows that thermalization of the models at 600 K produces

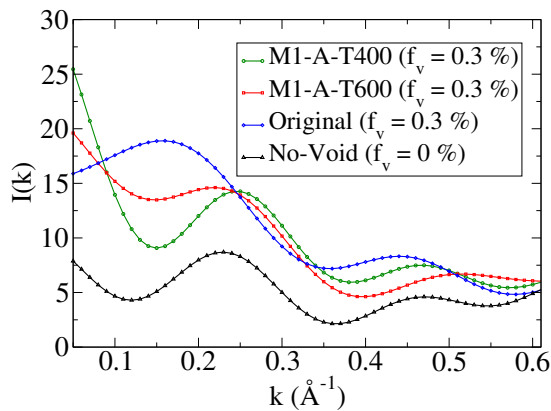


FIG. 4. The computed values of the scattering intensity from the original model (blue) before annealing and after annealing at 400 K (green) and 600 K (red). For comparison, the scattering intensity from the model with no voids (black) is also shown in the plot.

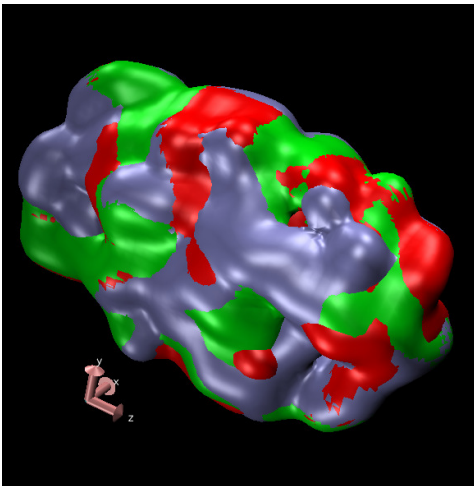


FIG. 5. The shape of the same ellipsoidal void obtained after relaxation of the annealed model (shown in Fig. 2) at 400 K (green) and 600 K (red).

considerable restructuring of void surfaces with atomic displacements of the surface atoms as high as 1.6 Å. The reconstruction of void surfaces has been found to be somewhat weakly reflected in one-dimensional scattering plots, obtained from the simulated values of the scattering intensity produced by the models. It has been observed that, despite considerable changes of void shape, one-dimensional measures of size, such as gyration and Guinier radii – obtained from the spa-

tial distribution of atoms and the intensity plots, respectively – are not particularly affected by low-temperature annealing.

ACKNOWLEDGEMENTS

This work is partially supported by U.S. National Science Foundation (NSF) under Grants No. DMR 1507166, No. DMR 1507118, and No. DMR 1506836.

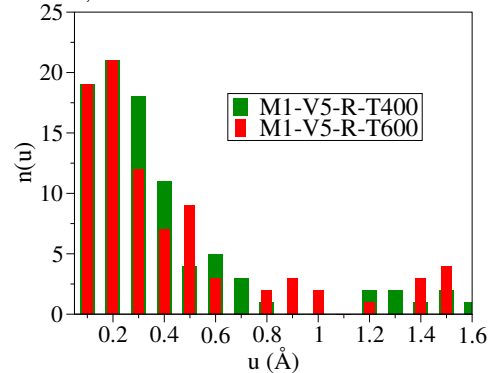


FIG. 6. The distributions of atomic displacements (u) of the atoms on the ellipsoidal void surface with the same color code as in Fig. 5. The symbol M1-V5-R-T400 signifies the relaxation of void number 5 in M1 model after annealing at 400 K.

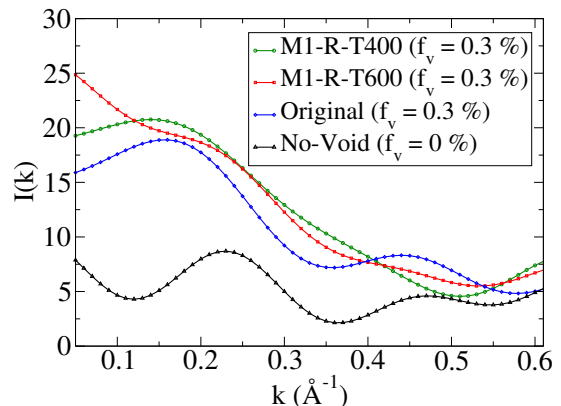


FIG. 7. The scattering intensities from the relaxed models after annealing at 400 K (green) and 600 K (red). The intensity values obtained from the original model with no voids (black) are also plotted for comparison.

REFERENCES

* Corresponding author: Partha.Biswas@usm.edu

¹ R. A. Street, *Hydrogenated Amorphous Silicon*, Cambridge Solid State Science Series (Cambridge University Press, 1991).

² M. H. Brodsky and R. S. Title, *Phys. Rev. Lett.* **23**, 581 (1969).

³ S. C. Moss and J. F. Graczyk, *Phys. Rev. Lett.* **23**, 1167 (1969).

⁴ A. H. Mahan, D. L. Williamson, B. P. Nelson, and R. S. Crandall, *Phys. Rev. B* **40**, 12024 (1989).

⁵ W. Liu, L. Zhang, F. Meng, W. Guo, J. Bao, J. Liu, D. Wang, and Z. Liu, *Scripta Materialia* **107**, 50 (2015).

⁶ W. Beyer, *Physica Status Solidi (c)* **1**, 1144 (2004).

TABLE II. Characteristic properties of void distributions in annealed models of *a*-Si. R_g , σ , and r_g indicate the average gyration radius, the root-mean-square fluctuation of R_g , and the Guinier radius from the scattering intensity plots in Fig. 4, respectively. A/R-T400 corresponds to the annealed/relaxed model at 400 K.

Models	$R_g \pm \sigma$ (Å)	r_g (Å)	Models	$R_g \pm \sigma$ (Å)	r_g (Å)
M1-A-T400	5.87±0.12	3.64	M1-R-T400	5.88±0.11	4.42
M1-A-T600	5.84±0.12	5.19	M1-R-T600	5.86±0.12	4.85
M2-A-T400	5.94±0.07	4.66	M2-R-T400	5.96±0.08	4.53
M2-A-T600	5.92±0.1	5.87	M2-R-T600	5.94±0.1	5.33

⁷ J. B. Boyce and M. Stutzmann, Phys. Rev. Lett. **54**, 562 (1985).

⁸ D. Paudel, R. Atta-Fynn, D. A. Drabold, S. R. Elliott, and P. Biswas, Phys. Rev. B **97**, 184202 (2018).

⁹ P. Biswas, D. Paudel, R. Atta-Fynn, D. A. Drabold, and S. R. Elliott, Phys. Rev. Applied **7**, 024013 (2017).

¹⁰ P. Biswas and S. R. Elliott, Journal of Physics: Condensed Matter **27**, 435201 (2015).

¹¹ P. Biswas, D. A. Drabold, and R. Atta-Fynn, Journal of Applied Physics **116**, 244305 (2014).

¹² R. B. Brahim and A. Chehaidar, Journal of Non-Crystalline Solids **357**, 2620 (2011).

¹³ Y. Hishikawa, Journal of Applied Physics **62**, 3150 (1987).

¹⁴ R. Vink, G. Barkema, W. van der Weg, and N. Mousseau, Journal of Non-Crystalline Solids **282**, 248 (2001).

¹⁵ J. Nocedal, Mathematics of Computation **35**, 773 (1980).

¹⁶ D. Williamson, A. Mahan, B. Nelson, and R. Crandall, Journal of Non-Crystalline Solids **114**, 226 (1989).

¹⁷ K. Laaziri, S. Kycia, S. Roorda, M. Chicoine, J. L. Robertson, J. Wang, and S. C. Moss, Phys. Rev. Lett. **82**, 3460 (1999).

¹⁸ W. Humphrey, A. Dalke, and K. Schulten, Journal of Molecular Graphics **14**, 33 (1996).

¹⁹ A. Guinier, *X-Ray Diffraction In Crystals, Imperfect Crystals, and Amorphous Bodies* (Dover Publications, Inc., New York, 1994).